



Block motion, slip rates, and earthquake hazard assessment of boundary faults in the Sichuan–Yunnan region, China

Changyun Chen¹ · Wei Zhan¹ · Xuechuan Li¹ · Shuang Zhu¹ · Qingyun Zhang¹ · Jingwei Li¹ · Nannan Guo¹ · Yi Tang¹

Received: 29 March 2023 / Accepted: 6 February 2024

© The Author(s) under exclusive licence to Institute of Geophysics, Polish Academy of Sciences 2024

Abstract

Quantitative analysis of the slip rate of active faults and their seismic parameters is important for seismic hazard analysis. In this study, we first construct an elastic block model to obtain the slip rate of boundary faults based on the distribution characteristics of active faults, seismicity, and global navigation satellite system (GNSS) observations in Sichuan–Yunnan, China. Then, the long-term seismic risks of the boundary faults are quantitatively evaluated based on the principle of seismic moment balance. The Sichuan–Yunnan region can be divided into 17 relatively independent and stable subblocks. There is clear zoning in the distribution and mechanisms of boundary fault movement and deformation. The boundary faults exhibit an alternating dextral–sinistral–dextral–sinistral strike-slip pattern from northeast to southwest. Among these boundary faults, the Xianshuihe–Xiaojiang fault zone has a high sinistral strike-slip rate, and the Jinshajiang fault plays an important role in accommodating the movement and deformation of the subblocks in the Chuandian block. The dextral strike-slip rate is approximately 10 mm/yr, which is diffusely transferred to the secondary boundary faults in the Chuandian block. Comparison of the rates of moment accumulation and release reveals that the southern segment of the Xiaojiang fault, the Longriba fault, the Daliangshan fault, and the Yuanmou fault exhibit significant moment deficits, with corresponding moment magnitudes exceeding M_w 7.5. More attention should be given to the strong earthquake risks of these faults. The Xianshuihe–Xiaojiang, Jiali–Lancangjiang, and Red River faults, which are arc shaped, dominate the regional deformation and determine the motion and deformation model of the subblocks and secondary boundary faults within the Chuandian block and the area southwest of the Red River fault.

Keywords Block division · Block motion · Slip rate · Earthquake hazard assessment · Global navigation satellite system (GNSS)

Introduction

Since the Cenozoic, the northward collision between the Indian and Eurasia plates has caused extensive uplift of the Tibetan Plateau (Armijo et al. 1989; Fielding 1996; Tapponnier et al. 2001). As the crust shortens and thickens (England and Molnar 2005), some of the plateau material is extruded to the periphery because of lower crustal flow (Clark and

Royden 2000). Global navigation satellite system (GNSS) data show that the southeastern segment of the Tibetan plateau is rotating clockwise around the Eastern Himalayan syntaxis (Wang et al. 2001; Gan et al. 2007). This large-scale movement has caused complex crustal deformation and intense seismic activity in and around the Tibetan Plateau. The Sichuan–Yunnan region located southeast of the Tibetan Plateau has become the front of the collision between the Indian and Eurasian plates. This region has a complex structure with frequent strong earthquakes. Therefore, quantitatively studying the crustal movement and deformation characteristics of the Sichuan–Yunnan region and the slip rates of the main active faults is important for elucidating the crustal deformation mechanism and analyzing the regional seismic risk of the Tibetan Plateau.

Edited by Dr. Rodolfo Console (ASSOCIATE EDITOR) / Prof. Ramón Zúñiga (CO-EDITOR-IN-CHIEF).

✉ Changyun Chen
chency@fmac.ac.cn

¹ The First Monitoring and Application Center, China Earthquake Administration, Tianjin 300180, China

The late Cenozoic and modern tectonic deformations in mainland China are characterized primarily by block motion, and strong earthquake activity is controlled by active block motion and concentrated at block boundaries (Zhang et al. 2003). The block motion characteristics in the Sichuan–Yunnan region are particularly prominent. Establishing a reasonable block model and studying the coordination and dynamic sources of the latest tectonic deformation characteristics for each block are important prerequisites for obtaining an in-depth understanding of regional crustal deformation patterns, lateral differences in seismic structures, temporal and spatial migration of strong earthquakes, regional earthquake hazards, and other scientific problems. In several previous studies, the Sichuan–Yunnan region was modeled with different blocks (Xu et al. 2003; Shen et al. 2005; Wang et al. 2008, 2001; Cheng et al. 2012; Li et al. 2021). These block models can be roughly classified into two types: those based on geological data and seismic activity (Xiang et al. 2000; Xu et al. 2003) and those based on fault geometry and geodetic data (Wang et al. 2001, 2017; Shen et al. 2005; Cheng et al. 2012; Li et al. 2021). There are limitations associated with both types of models. In the former type, the large number of faults makes it difficult to select the most reasonable fault as the boundary. In the latter type, the primary consideration is the spatial distribution of GNSS stations, with less consideration of structural factors. This study provides a comprehensive analysis of the distribution characteristics of regional active tectonics and seismicity to propose a block partitioning scheme for the Sichuan–Yunnan region. An analysis of the stability and independence of the partition results yields the latest block model. Based on this latest block model, GNSS geodetic data and an elastic block model are used to invert the motion characteristics of block boundary faults, and an analysis is performed on the long-term seismic hazards of the boundary faults, the distribution characteristics of regional deformation, and the main dynamic sources of current crustal deformation.

Tectonic setting

Strong earthquakes occur frequently in the Sichuan–Yunnan region in the southeastern part of the Tibetan Plateau (Fig. 1). The ongoing northward push of the Indian plate explains much of the modern crustal deformation and seismicity in the Sichuan–Yunnan region (Tapponnier et al. 2001). Active faults with various strike-slip rates, sizes, and mechanical properties control the modern crustal deformation and distribution of large earthquakes (Xu et al. 2003; Lee and Lawver 1995) and divide this region into several tectonic terranes or subblocks (Xu et al. 2003).

The sinistral Xianshuihe–Xiaojiang fault zone forms the boundary among the Bayan Har, Chuandian, and South

China blocks. The Xianshuihe–Xiaojiang fault zone is composed of three sections. The northern section is the Xianshuihe fault, the middle section features the Anninghe and Zemuhe faults, and the southern section is the Xiaojiang fault. The Daliangshan and Mabian faults lie east of the Anninghe and Zemuhe faults (He et al. 2008). The strike-slip rates decrease significantly along the Anninghe and Zemuhe faults in the middle part of the Xianshuihe–Xiaojiang fault zone. The Xianshuihe and Xiaojiang faults both have left-lateral strike-slip rates of approximately 15 mm/yr (Allen et al. 1991; He et al. 2006; He and Oguchi 2008), whereas the slip rates along the Anninghe and Zemuhe faults are approximately 3–7 mm/yr and 5–8 mm/yr (He and Oguchi 2008), respectively. The missing slip rate is thought to be accommodated by the Daliangshan and Mabian faults, east of the Anninghe and Zemuhe faults (He et al. 2008).

The eastward motion of the Bayan Har block is obstructed by the stable Sichuan Basin and is mainly partitioned into uplift along the Longmenshan and Minshan faults, and dextral motion across the Longriba and Longmenshan faults (Ren et al. 2013). The elevation of the eastern margin of the Bayan Har block is approximately 6500 m; to the east, the elevation of the Sichuan Basin is no more than 500 m (Shen et al. 2005). The extensive and rapid uplift of the eastern margin of the Bayan Har block resulted from material flow and extrusion from the interior of the Tibetan Plateau to the east and southeast (Yan et al. 2010).

The dextral strike-slip Red River fault is the southeastern boundary of the Chuandian and Dianmian blocks. This fault with strong linear characteristics can be easily found in satellite images (Allen et al. 1984; Tapponnier et al. 1990). The dextral offset is estimated to be approximately 6–60 km (Allen et al. 1984; Wang 1998). The northwestern end of the Red River fault intersects with the Weixi–Qiaohou fault, which trends NW; the Zhongdian–Daju fault, which trends nearly north–south; and the Lijiang–Xiaojinhe fault, which trends NE. The Lancangjiang and Nujiang faults lie west of the Weixi–Qiaohou fault. The northern and southern ends of the Nujiang fault intersect with the Jiali and Longling–Ruili faults, respectively. The Nantinghe and Menglian faults are parallel to the Longling–Ruili fault to the southeast. The Jinshajiang fault lies north of the Zhongdian–Daju fault and is the boundary between the Qiangtang and Chuandian blocks. In addition to several historical strong earthquakes (Department of Earthquake Disaster Prevention, China Earthquake Administration 1999), more than 15 M6 events have occurred along these faults since 1976 (Department of Earthquake Disaster Prevention, State Seismological Bureau 1995; The Working Group of M7 2012).

Over the past three decades, Earth observation technology, including GNSSs, has developed at a rapid pace and can provide efficient, reliable, and accurate observation results for monitoring crustal deformation processes at different

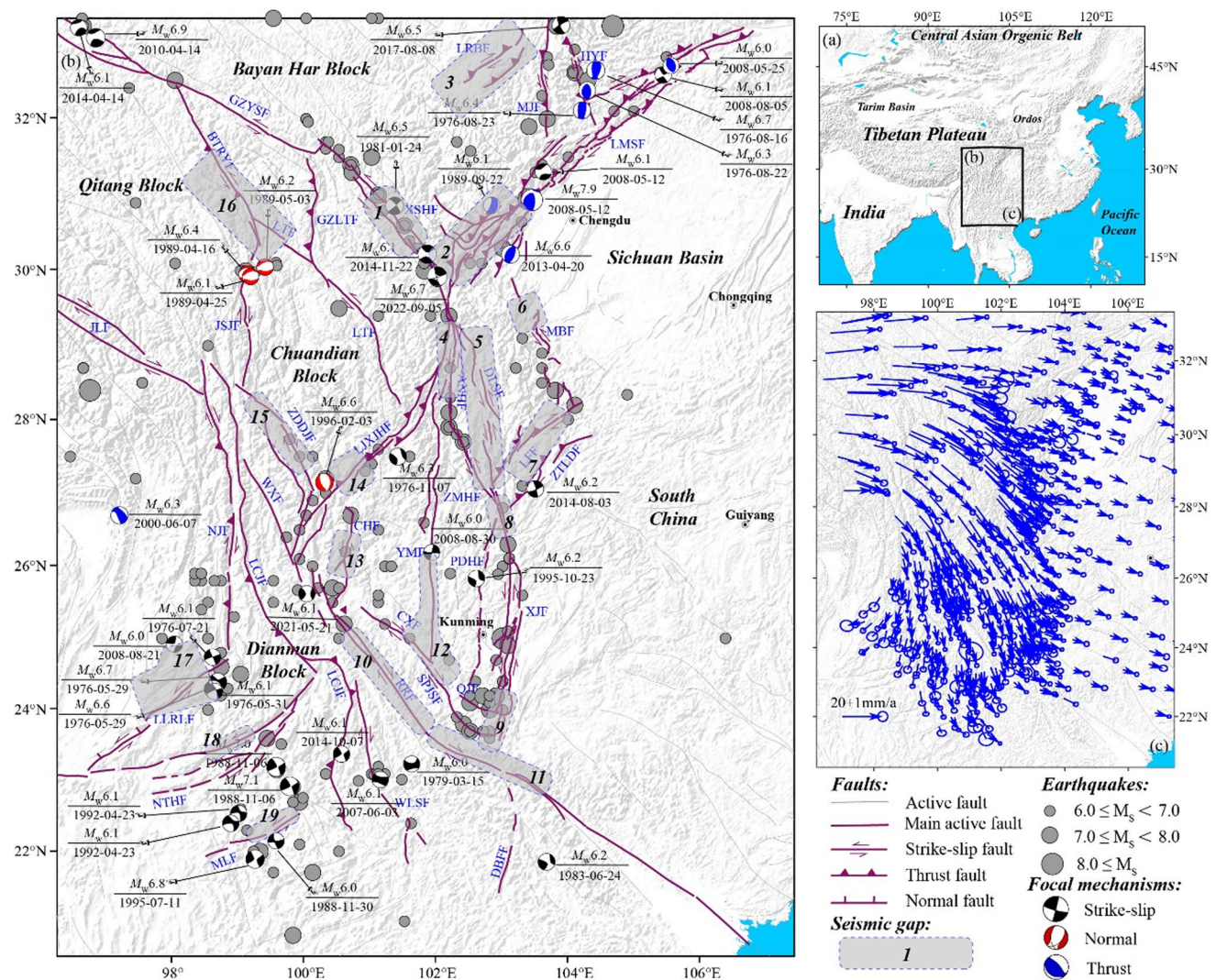


Fig. 1 **a** Index map of the study area; **b** major active faults, strong earthquakes, and seismic gaps in the Sichuan–Yunnan region. The focal mechanism ($M_w \geq 6.0$) data were obtained from the Global Centroid Moment-Tensor Project (GCMT; <https://www.globalcmt.org>); the gray filled circles represent historical earthquakes of $M \geq 6.0$ (Department of Earthquake Disaster Prevention, State Seismological Bureau 1995; Department of Earthquake Disaster Prevention, China Earthquake Administration 1999); the gray areas (1–19, where details are provided in the Supporting Information Text S1) surrounded by dashed lines represent seismic gaps (The Working Group of M7 2012). **c** GNSS horizontal velocity field in the Sichuan–Yunnan region (Kreemer et al. 2014; Wang and Shen 2020) with respect to the Eurasian plate. Fault names: ANHF Anninghe fault, BTRYF

Batang–Riyu fault, CHF Chenghai fault, CXF Chuxiong fault, DLSF Daliangshan fault, DBFF Dian Bien Phu fault, HYF Huya fault, GZYSF Ganzi–Yushu fault, GZLTF Ganzi–Litang fault, JLF Jiali fault, JSJF Jinshajiang fault, LCJF Lancangjiang fault, LFF Lianfeng fault, LJXJHF Lijiang–Xiaojinhe fault, LLRLF Longling–Ruili fault, LMSF Longmenshan fault, LTF Litang fault, LRBFF Longriba fault, MBF Mabian fault, MJF Minjiang fault, MLF Menglian fault, NJF Nujiang fault, NTHF Nantinghe fault, PDHF Puduhe fault, QJF Qujiang fault, RRF Red River fault, SPJSF Shiping–Jianshui fault, XJF Xiaojiang fault, XSHF Xianshuihe fault, WLSF Wuliangshan fault, WXF Weixi–Qiaohou fault, YMF Yuanmou fault, ZDDJF Zhongdian–Daju fault, ZMHF Zemuhe fault, ZTLDF Zhaotong–Ludian fault

scales and for monitoring the motion and deformation characteristics of active faults (Kong et al. 2019; Botsyo et al. 2020; Liu et al. 2021). Earth observation technology has become an important technical means of studying plate tectonics, regional crustal motion and deformation modes, active fault activity characteristics, earthquake monitoring and forecasting, etc. The valuable GNSS observations produced by the Crustal Movement Observation Network of

China (CMONOC) and the Continental Tectonic Environment Monitoring Network of China (CTEMNC) (Wang et al. 2001; Shen et al. 2005; Gan et al. 2007; Liang et al. 2013; Zheng et al. 2017; Wang and Shen 2020; Tao et al. 2021; Su et al. 2023) provide high-precision, high spatial–temporal resolution, and highly reliable data for studying the characteristics of regional crustal deformation and seismogenic processes of strong earthquakes (Wu et al. 2015). The

GNSS velocities clearly show that the crustal motion in the Sichuan–Yunnan region clockwise around the Eastern Himalayan syntaxis (Fig. 1c).

Block divisions and the independence test

Block divisions

Active blocks result from local deformation of the brittle crust during neotectonics and are tectonic units that are cut and bounded by late Quaternary active structures that are still active today (Zhang et al. 2003). Active block motion occurs through seismic or nonseismic fracturing and frictional sliding of different types of active boundary tectonic zones, especially active faults, as well as plastic deformation within a narrow spatial range of the boundary. Block boundary faults control the spatial distribution of historical, present, and future damaging earthquakes. (Nur et al. 1989; Xu et al. 2003). An independent active block is a tectonic domain with well-defined size, consistent kinematic characteristics, little internal deformation, and weak seismicity. An active block is surrounded by different types of active faults or seismic zones that are kinematically coordinated with each other (Nur et al. 1989). In this study, to obtain reasonable block partitioning results, active subblocks in the Sichuan–Yunnan region are finely divided based on the geometric characteristics of major active faults and seismicity. The stability of the blocks was analyzed in terms of the residual distribution characteristics determined using a rigid block model. The independence between two neighboring blocks is analyzed by the F test method (Wang et al. 2003).

The residual velocities between the GNSS velocity and model velocity can be used to analyze the rationality of the block partitioning results (Wang et al. 2003; Shen et al. 2005; Chen et al. 2013). Randomly distributed residual velocities represent permanent deformation in the region, indicating reasonable block division. Regularly distributed residual velocities inside a block indicate that further division is needed. Wang and Shen. (2020) obtained relatively abundant GNSS velocity field data in the study area by deducing coseismic and postseismic deformations and considering solutions from other studies (Kreemer et al. 2014). Therefore, in this study, a portion of the velocity field of 528 GNSS stations (Fig. 1c) in the Sichuan–Yunnan region was taken from Wang and Shen (2020) and used to analyze the rationality of block division.

According to the aforementioned principles, we divided the Sichuan–Yunnan region into two levels of active blocks: first-grade blocks and subblocks within the first-grade blocks. In previous studies, the boundaries of the first-grade blocks were delineated and the Sichuan–Yunnan

region was divided into five first-grade active blocks, i.e., Bayan Har, South China, Chuandian, Qiangtang, and Dianmian (Xu et al. 2003; Zhang et al. 2003; Shen et al. 2005). The division of the subblocks within the Bayan Har and South China blocks is relatively clear. The Bayan Har block is bounded by the Longmenshan, Ganzi–Yushu and Xianshuihe faults. The Longriba fault, parallel to the Longmenshan fault, is located in the Bayan Har block and divides it into the Aba and Maerkang subblocks (Xu et al. 2003; Shen et al. 2005; Chen et al. 2013). The South China block is bounded by the Longmenshan, Anninghe, Zemuhe and Xiaojiang faults. It can be divided into the Daliangshan, Mabian and Huanan subblocks (Wang et al. 2008). The Daliangshan subblock, is bounded by the Daliangshan fault in the east, the Anninghe fault in the northwest and the Zemuhe fault in the southwest. To the east is the Mabian subblock, bounded by the Longmenshan fault to the north, the Daliangshan fault to the west, the Lianfeng fault to the south, and the Mabian fault to the east. The Huanan subblock is bounded by the Longmenshan fault to the north and the Mabian and Xiaojiang faults to the west. The Chuandian block is divided into two subblocks by the Lijiang–Xiaojinhe fault, i.e., the Dianzhong and Diannan subblocks (Xu et al. 2003; Wang et al. 2008, 2021; Li et al. 2021). The Dianzhong and Diannan subblocks can be further divided considering internal faults and seismicity. In previous studies, the Dianzhong subblock was divided into three subblocks by the Litang and Zhongdian–Daju faults, i.e., the Litang, Daocheng, and Weixi subblocks (Xu et al. 2003; Shen et al. 2005). The Litang subblock is bounded by the Xianshuihe fault on the east, the Litang fault in the west, the Lijiang–Xiaojinhe fault in the south, and the Batang–Riyu fault in the northwest. The Daocheng subblock is located west of the Litang subblock; and is bounded by the Jinshajiang, Zhongdian–Daju, Lijiang–Xiaojinhe and Litang faults. The Weixi subblock is located west of the Daocheng subblock and is bounded by the Zhongdian–Daju, Weixi–Qiaohou, and Lijiang–Xiaojinhe faults.

The division of subblocks within the Diannan subblock is controversial. The major faults in the Diannan subblock are the N–S-trending Chenghai, Yuanmou, and Puduhe faults and the NW-trending Qujiang, Chuxiong, and Shiping–Jianshui faults (Fig. 1). No objections have been put forward regarding assigning the Chenghai fault as the eastern boundary of the Chenghai subblock, which has been supported by many studies (Xu et al. 2003; Wang et al. 2008, 2021; Li et al. 2021). However, there is debate about whether the Yuanmou, Puduhe, Chuxiong, and Shiping–Jianshui faults can be used as the boundaries of subblocks and whether it is more reasonable to use the eastern or western branch of the Xiaojiang fault as the block boundary. The residual distribution characteristics reveal clear deformation of the Diannan

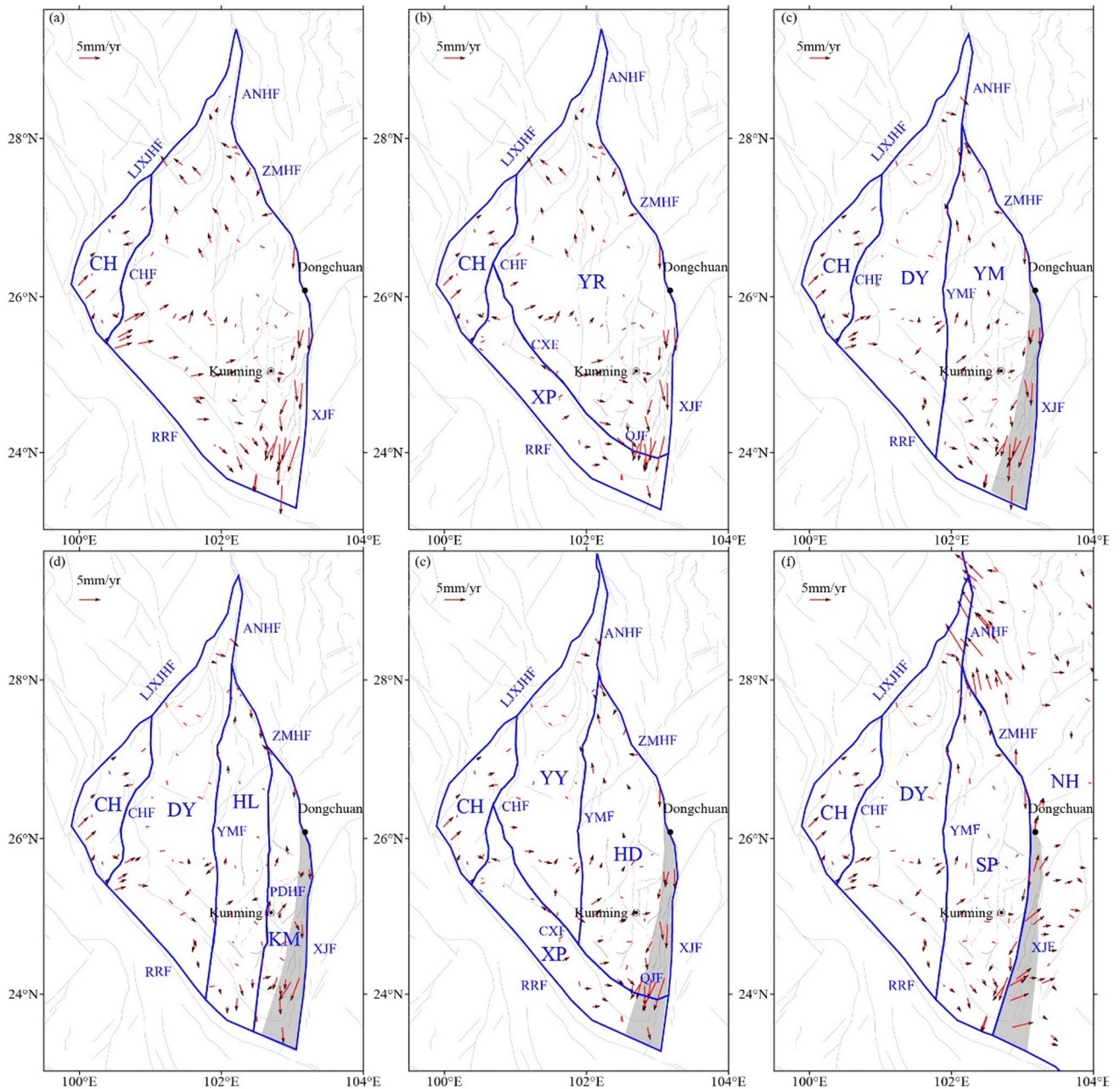


Fig. 2 Block partitioning schemes for the region west of the Xiaojiang fault. CH, YR, XP, DY, YM, HL, KM, YY, HD, NH, and SP represent the Chenghai, Yongren, Xiping, Dayao, Yimen, Huili, Kunming, Yanyuan, Huidong, Nanhua, and Shipping subblocks, respectively. **a** Using the Chenghai fault, southeastern segment of the Lijiang–Xiaojinhe fault and northwestern segment of the Red River fault as the boundaries of the CH subblock; **b** using the Chuxiong fault, the Qujiang fault, southwestern segment of the Chenghai fault, southern segment of the Xiaojiang fault, and the middle and southeastern segments of the Red River fault as the boundaries of the XP subblock; and using the Chuxiong, Qujiang, Anninghe, Zemuhe, Xiaojiang, Lijiang–Xiaojinhe, and Chenghai faults as the boundaries of the YR subblock; **c** using the Zemuhe fault, the eastern branch

of the Xiaojiang fault, the Yuanmou fault and southeastern segment of the Red River fault as the boundaries of the YM subblock; and using the Yuanmou fault, the Chenghai fault, northeastern segment of the Lijiang–Xiaojinhe fault and middle segment of the Red River fault as the boundaries of the DY subblock; **d** using the Huili fault to divide the YM subblock into HL and KM subblocks; **e** using the Chuxiong fault to divide the DY and YM subblocks into the YY, HD, and XP subblocks; **f** using the western branch of the Xiaojiang fault as the boundary of the SP subblock; and using the Anninghe fault, the Zemuhe fault and the western branch of the Xiaojiang fault as the boundaries of the NH subblock. The fault abbreviations used here are the same as those in Fig. 1

subblock east of the Chenghai subblock (Fig. 2a). Therefore, several different block models are proposed in this study to explain these deformation characteristics. First, we consider the Chuxiong and Qujiang faults as subblock boundaries to divide the region east of the Chenghai subblock into two subblocks, the Yongren and Xinping subblocks (Fig. 2b). There are no significant changes in the residual characteristics of these subblocks, especially for the Yongren subblock. Then, we attempt to use the Yuanmou fault as a subblock boundary to divide the region east of the Chenghai subblock into two subblocks, the Dayao and Yimen subblocks (Fig. 2c). To the northwest of Dongchuan city, the Xiaojiang fault splits into two branches, one in the east and one in the west. There has been significant improvement in areas other than that between the two branches of the Xiaojiang fault. We propose several block partitioning schemes to explain the deformation characteristics of the residual distribution in the southern section of the Xiaojiang fault. We attempt to divide the Yimen subblock into two subblocks, i.e., Huili and Kunming, by first using the Puduhe fault as the boundary (Fig. 2d) and then using the Chuxiong and Qujiang faults as subblock boundaries to divide the region east of the Chenghai subblock into three subblocks: Xinping, Yanyuan, and Huidong (Fig. 2e). In addition, the western branch of the Xiaojiang fault could be used as the eastern boundary of the Diannan subblock (Fig. 2f). All the aforementioned subblock partitioning results show that the various considered block division methods cannot effectively explain the local deformation of the southern end of the Xiaojiang fault. Considering that the stations associated with large residual errors are primarily distributed between two branches of the Xiaojiang fault, we propose that this local deformation corresponds to interior deformation of the Xiaojiang fault and that the Yimen subblock should not be further divided. Our model is consistent with the distribution of metamorphic belts and main types of metamorphism in Yunnan Province (Bureau of Geology and Mineral Resources of Yunnan Province, 1990).

Southwest of the Red River fault is the Dianmian block, and the tectonic deformation and distribution of strong earthquakes in the region are mainly controlled by the Lancangjiang, Nujiang Longling–Ruili, Nantinghe, and Menglian faults (Fig. 1). Among these faults, the NW-trending Lancangjiang fault plays an extremely important role in subblock division. The two sides of the Lancangjiang fault represented zones of subsidence and uplift in the Cretaceous (Bureau of Geology and Mineral Resources of Yunnan Province, 1990), and the tectonic features of the two sides are obviously different; therefore, we divide the Dianmian block into two subblocks separately by the Lancangjiang fault. More faults are located south of the Lancangjiang fault than north of it, including the NW-trending Nujiang fault and a series of NE-trending faults, i.e., the Longling–Ruili, Nantinghe, and Menglian faults (Fig. 1).

Therefore, we use the Lancangjiang, Longling–Ruili, Nantinghe, and Menglian faults as boundaries to divide the Dianmian block into five subblocks, i.e., the Tengchong, Baoshan, Jinggu, Menglian, and Simao subblocks (Fig. 3). The Simao subblock is bounded by the Red River fault to the north and the Lancangjiang fault to the south. The Tengchong subblock is bounded by the Longling–Ruili fault to the southeast, the Nujiang fault to the east, and the Jiali fault to the north. Southeast of the Tengchong subblock, bounded by the Longling–Ruili, Nantinghe, and Lancangjiang faults, is the Baoshan subblock. The Jinggu subblock is located southeast of the Baoshan subblock and is bounded by the Nantinghe, Menglian, and Lancangjiang faults. The Menglian subblock is bounded by the Lancangjiang and Menglian faults. The subblock model is in good agreement with previous delineation results (Shen et al. 2002; Liu et al. 2020).

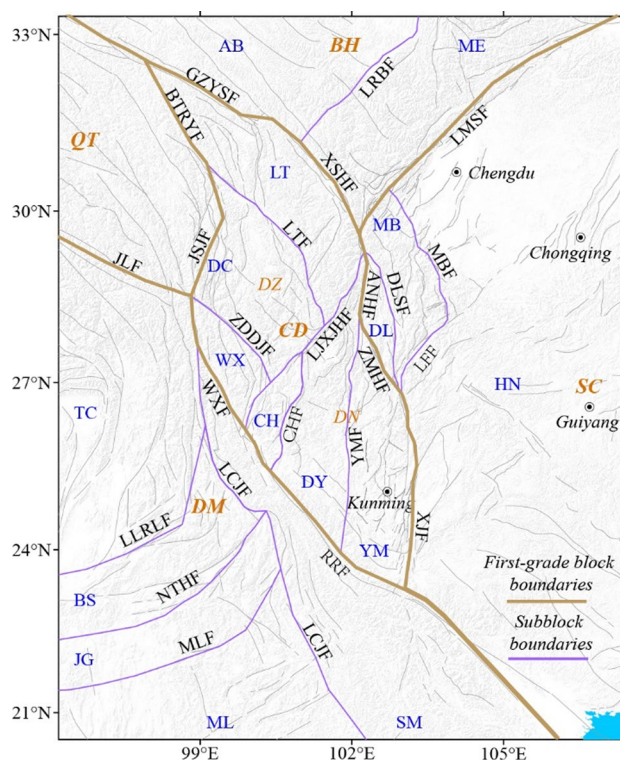


Fig. 3 Block model of the Sichuan–Yunnan region. *BH* Bayan Har block, *AB* Aba subblock, *MK* Maerkang subblock, *SC* South China block, *DL* Daliangshan subblock, *DN* Diannan subblock, *DZ* Dianzhong subblock, *MB* Mabian subblock, *HN* Huanan subblock, *CD* Chuandian block, *DC* Daocheng subblock, *LT* Litang subblock, *WX* Weixi subblock, *CH* Chenghai subblock, *DY* Dayao subblock, *YM* Yimen subblock, *QT* Qiangtang block, *DM* Dianmian block, *TC* Tengchong subblock, *BS* Baoshan subblock, *JG* Jinggu subblock, *ML* Menglian subblock, *SM* Simao subblock. The fault abbreviations used here are the same as those in Fig. 1

Independence testing of active subblocks

Following the preliminary division of the active subblocks, the F test was used to assess the independence between adjacent blocks (Wang et al. 2003). First, we compute the Euler rotation poles of two neighboring blocks, and their fitting residual Chi-squares are x_1^2 and x_2^2 . Then, we assume that the neighboring two blocks are one, and the fitting residual Chi-square is x_{12}^2 . The F value can be calculated by the following formula:

$$F = F(x_{12}^2, 2n_1 + 2n_2 - 3, x_1^2 + x_2^2, 2n_1 + 2n_2 - 6) \\ = x_{12}^2(2n_1 + 2n_2 - 6) / (x_1^2 + x_2^2)(2n_1 + 2n_2 - 3), \quad (1)$$

where n_1 , n_2 and n_{12} are the numbers of GNSS sites located in the adjacent blocks and the merged blocks, respectively. The significance level is evaluated by $F \times 100\%$. We repeat the calculation of the F value for all neighboring pairs of blocks, until all of their significance levels are above a criterion value of 100%. The testing process was conducted in three steps. First, the mutual independence of two neighboring first-grade blocks, i.e., Bayan Har, South China, Chuandian, Qiangtang, and Dianmian, was tested. The results (Table S1) show that the significance of mutual independence between adjacent blocks is 100%, indicating that the first-grade blocks are independent of each other. The independence of the two neighboring subblocks of the Chuandian block, i.e., the Dianzhong and Diannan subblocks, was subsequently studied (Table S2). Finally, the mutual independence among the subblocks of the Dianzhong subblock, Diannan subblock, Dianmian block, and South China block was tested and found to have a significance of 100% (Table S1). The F test results demonstrated that the Aha and Maerkang subblocks within the Bayan Har block are completely independent (Chen et al. 2013).

Block motion and boundary fault slip rate

Block motion

An analysis of the geometric distributions of active faults, strong earthquakes, crustal deformation characteristics reflected by GNSS observation data, geophysical field data, etc., is used to construct a detailed subblock division scheme for the Sichuan–Yunnan area. Assuming that each subblock is approximately rigid, has little or no internal deformation, and has deformation that is mainly concentrated at the boundary faults, the rigid motion characteristics of each block are calculated using the GNSS velocity field under the Eurasian framework. The results show that each block rotates while undergoing translational motion (Fig. 4a). The

surface velocities produced by the rigid block model used in this study agree well with the GNSS velocity fields (Fig. 4b). Overall, the rotation rate of the subblocks decreases from northwest to southeast. The results of the relative motion among the subblocks show that the eastward component of the translational motion rate of each subblock in the Chuandian block is greater than those of the Dianmian blocks to the southwest (Fig. 4c). The southward component of the translational motion rate of each subblock in the Chuandian block is clearly larger than those of the Baya Har, South China and Dianmian blocks on both sides (Fig. 4d). The rate of translational motion of the subblocks within the Chuandian block decreases from the northwest to the southeast.

In the ideal case in which the medium properties of the block can be neglected, the fitting residual of the active block motion primarily comprises two parts: the observation error corresponding to the block interior and the part reflecting the block deformation characteristics after deducting the observation error, namely, the degree of block deformation. Data from singular stations are removed when calculating block motion, such that the observation error can be treated as a systematic error that does not affect the comparison of relative deformation differences between subblocks. The residual distributions are normal and relatively narrow (Fig. 5a), indicating that each subblock interior is relatively stable. In general, the velocity residual components follow a normal distribution in the eastward and northward directions (Fig. 5b, c), and approximately 81% of the residual velocity magnitude is no more than 2 mm/yr.

Fault slip rate

A linear spherical block (Meade and Loveless 2009) was developed to analyze the regional kinematics and fault slip rates in the Yunnan–Sichuan region. Within this model, all faults are assumed to be locked during an interseismic period. The interseismic velocity V_I is constrained by the GNSS velocities and can be defined as $V_I = V_B(\Omega) - V_{\text{CSD}}(\Omega)$, where Ω is the Euler vector for the block rotation; V_B is the long-term relative block motion; and V_{CSD} is the deficit slip rate due to fault locking, which can be obtained by using an elastic half-space model (Okada 1985) and corresponds well to the long-term geological slip rate of the fault (Savage and Burford 1973). The simulated rate throughout the whole interseismic period at a point is equal to the sum of the block rotation rate, the accumulation of elastic strain at all faults, and the uniform elastic strain inside the block (Meade and Loveless 2009). Within this model, the rigid rotation and deficit slip rate of the fault during the interseismic period are calculated based on GNSS data (Savage and Burford 1973). A uniform dip of 90° has typically been used in previous studies (Meade 2007; Li et al. 2021; Wang et al. 2021) and is employed in our model. The

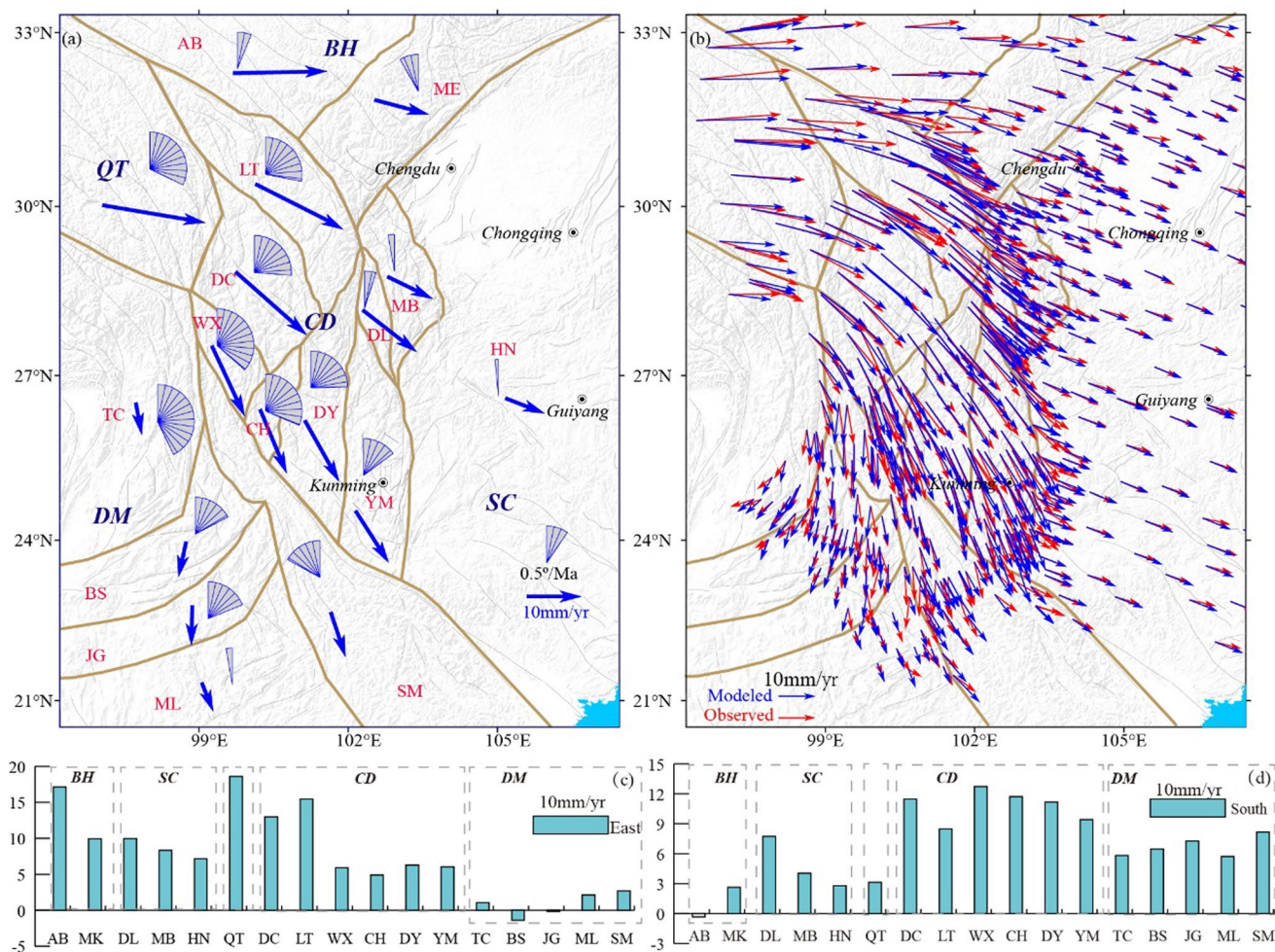


Fig. 4 **a** Translational and rotational motion of the active subblocks in the Sichuan–Yunnan region with respect to the Eurasian plate. **b** The modeled velocities and GNSS site velocities are indicated by

blue and red arrows, respectively. The eastward **c** and southward **d** components of the translational motion rates of the subblocks in the Sichuan–Yunnan region

locking depth is an important parameter for the inversion process. The locking depth is uniformly taken as 15 km by considering seismic relocation results (The Working Group of M7 2012), the depth of modern destructive earthquakes (Li et al. 2012; Yi et al. 2017), and the optimal locking depth of major faults in the Sichuan–Yunnan region (Wang et al. 2011, 2022; Zhao et al. 2020). Figure 6 shows the strike-slip and compressive/tensile rates of the major faults in the study area.

Slip rates along the Longmenshan and Longriba faults

The Longmenshan fault is located in the eastern part of the Tibetan Plateau and generated the M_w 7.9 Wenchuan earthquake on May 12, 2008 (Zhang et al. 2008). Preseismic GNSS observations (Zhang et al. 2008), seismic and geological studies (Tang and Han 1993; Densmore et al. 2007; Zhou et al. 2007; Wen et al. 2009, 2011; Xu et al. 2017), and

historical seismic records (Wen et al. 2009, 2011) indicate a very low strike-slip rate for the Longmenshan fault of no more than 1 mm/yr (Ma et al. 2005; Densmore et al. 2007). Our results show that the dextral strike-slip rate along the Longmenshan fault is 0.3 ± 0.1 mm/yr, consistent with the results of previous studies (Tang and Han 1993; Ma et al. 2005; Densmore et al. 2007; Zhou et al. 2007; Wen et al. 2011, 2009).

The Longriba fault is parallel to the NE-trending Longmenshan fault and lies in the eastern part of the Tibetan Plateau. Shen et al. (2005) analyzed the GNSS velocity with respect to the Sichuan Basin and found clear gradients, resulting in speculation about the existence of the Longriba fault (Shen et al. 2005). Xu et al. (2008) verified the GNSS results through a satellite field investigation and image interpretation and determined a dextral strike-slip rate of 5.4 ± 2.0 mm/yr in the northeastern section of the Longriba fault since the late Pleistocene (Xu et al. 2008). The latest

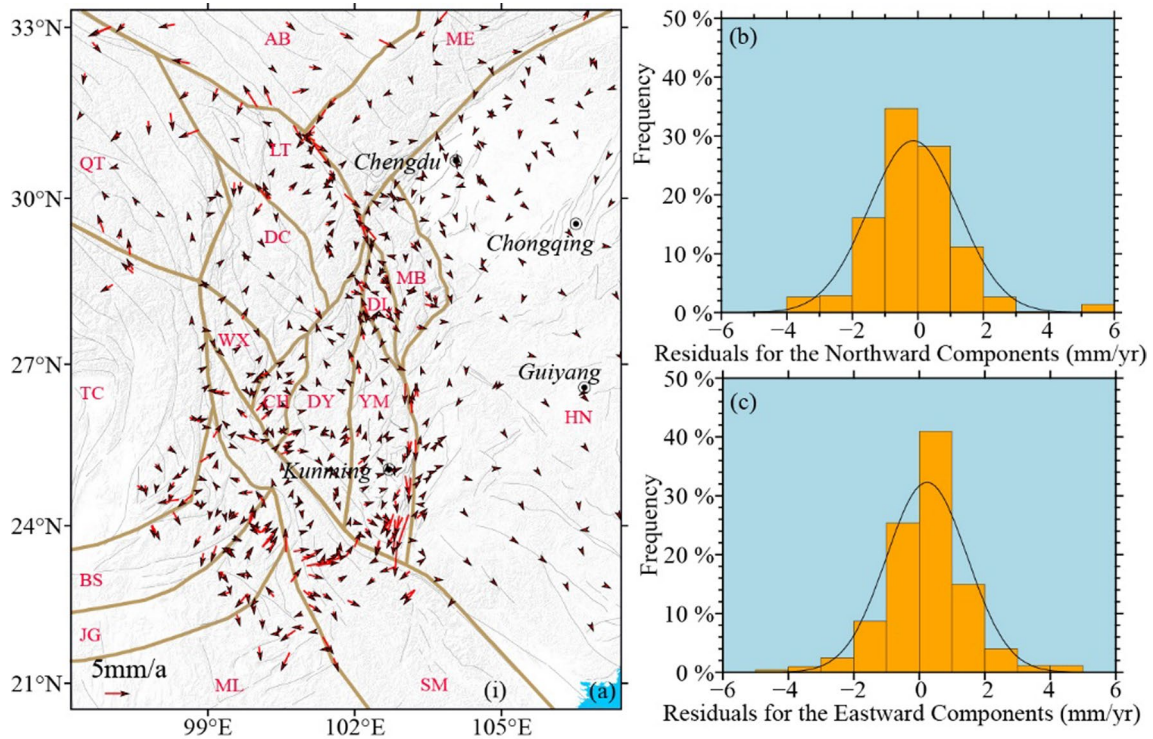


Fig. 5 The residual velocity distribution (a) and histogram statistics of the modeling residual velocities for the northward (b) and eastward (c) components

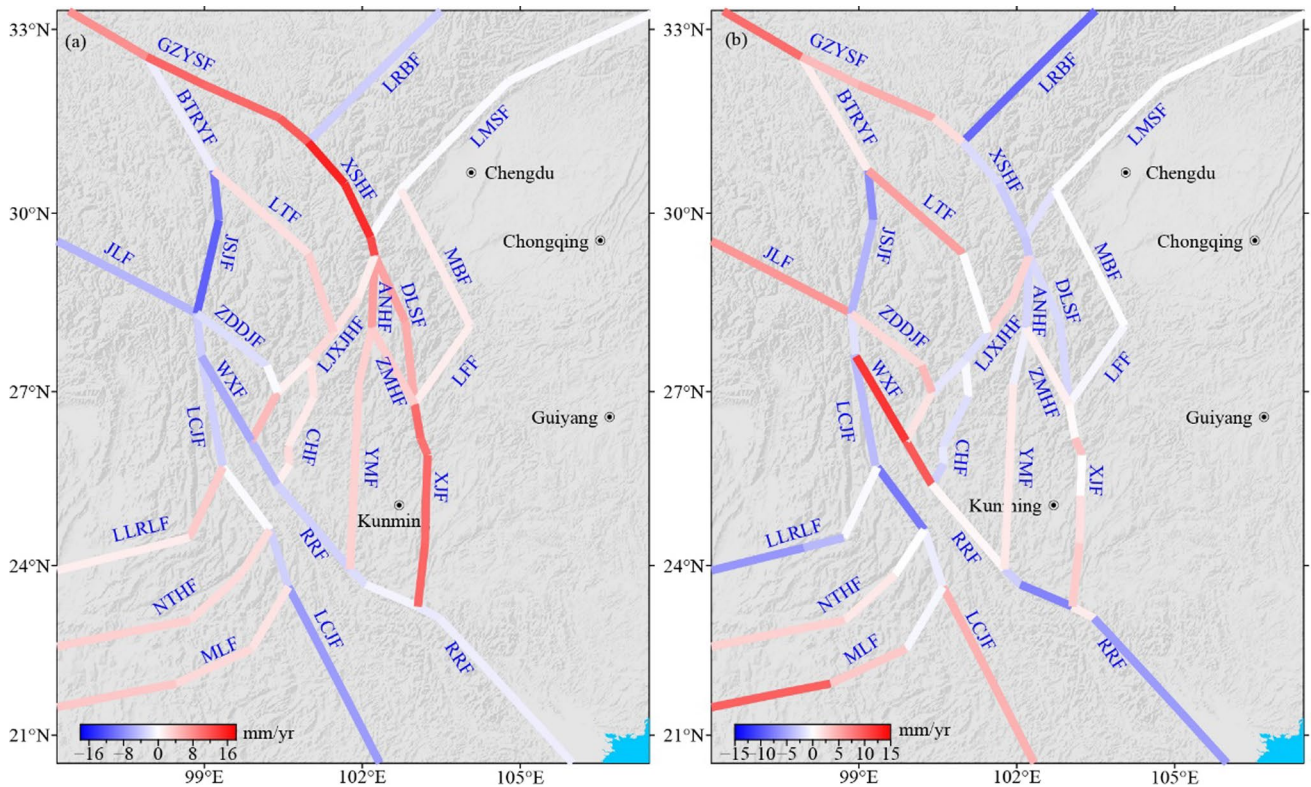


Fig. 6 The sinistral (red)/dextral (blue) strike-slip rates and tensile (red)/compressive (blue) slip rates along the major faults in the Sichuan–Yunnan region

seismic survey results suggest that the dextral strike-slip rate of the Longriba fault decreased from approximately 7.5 mm/yr in the latest Pleistocene to 2.1 mm/yr in the Holocene (Ren et al. 2013). The dextral strike-slip rate of the Longriba fault determined in this study is 3.5 ± 0.4 mm/yr, which is slightly greater than the Holocene slip rate and less than the Pleistocene slip rate.

Fault slip rates in and around the Chuandian block

The eastern boundary of the Chuandian block is composed of the Ganzi–Yushu and Xianshuihe–Xiaojiang fault zones. Geological studies based on low-resolution geomorphic markers and imprecise or relative dating techniques yielded a large range of 3 mm/yr to 14 mm/yr for the sinistral slip rate along the Ganzi–Yushu fault (Wen et al. 2003; Peng et al. 2006). Based on GNSS data, a short-term strike-slip rate in the range of 10–16 mm/yr was reported (Shen et al. 2005). Our results show an increase in the sinistral strike-slip rate from 7.8 ± 0.3 mm/yr in the northwestern segment of the Ganzi–Yushu fault to 10.7 ± 0.3 mm/yr in the southeastern segment. Previous studies based on geomorphologic offsets and dating techniques have shown that the strike-slip rate of the Xianshuihe fault is approximately 15 mm/yr (Allen et al. 1991; Xu et al. 2003). Geodetic studies yield strike-slip rates ranging widely from 9–16 mm/yr (Loveless and Meade 2011; Wang et al. 2017). Our results show that the sinistral strike-slip rates from northwest to southeast along the Xianshuihe fault are 11.5 ± 0.2 mm/yr, 15.2 ± 0.2 mm/yr, and 12.8 ± 0.2 mm/yr. The slip rate along the northwestern segment of the Xianshuihe fault agrees well with the InSAR-observed rate of approximately 10.5 mm/yr (Wang et al. 2009), and the results for other segments are consistent with those of recent GNSS studies (Li et al. 2021; Wang et al. 2021).

The N–S-trending Anninghe fault lies south of the Xianshuihe fault and is approximately 160 km long. Our model results indicate a strike-slip rate of 6.7 ± 0.3 mm/yr for the Anninghe fault. The Zemuhe fault lies south of the Anninghe fault and has a sinistral strike-slip rate of 3.5 ± 0.3 mm/yr. The Daliangshan and Mabian faults lie east of the Anninghe and Zemuhe faults and absorb the remaining sinistral strike-slip motion, resulting in rates of approximately 6.1 mm/yr and 1.4 mm/yr, respectively. These results are in good agreement with previous geodetic (Shen et al. 2005; Li et al. 2021) and geological (Tang and Han 1993; Ren 1994; Xu et al. 2003; He and Oguchi 2008; Wei et al. 2012) studies. The Xiaojiang fault lies south of the Zemuhe and Daliangshan faults. The sinistral strike-slip rate of the Xiaojiang fault is 10.5 ± 0.1 mm/yr, which is consistent with the geological result of 10 ± 2 mm/yr (Song et al. 1998).

Our model was used to divide the Red River fault into six segments with dextral strike-slip rates from northwest to southeast of 4.9 ± 0.5 , 3.2 ± 0.2 , 2.4 ± 0.2 , 0.8 ± 0.2 , 1.5 ± 0.1 , and 1.2 ± 0.1 mm/yr. The average slip rates of the three segments in the southeastern part of the Red River fault are close to previous values (Allen et al. 1984; Xu et al. 2003; Trinh et al. 2012). The segment northwest of the intersection between the Red River and Xiaojiang faults exhibits a high shortening rate of 7.2 ± 0.2 mm/yr. The Zhongdian–Daju fault lies north of the Red River fault and has a dextral strike-slip rate of 2.3 ± 0.3 mm/yr, which is in good agreement with the Quaternary slip rate determined by geological studies (Replumaz and Tapponnier 2003). The Jinshajiang fault lies north of the Zhongdian–Daju fault, and comprises several secondary faults, with a dextral strike-slip rate of 3.5–7 mm/yr (Tang and Han 1993; Chang et al. 2015). In our model, the Jinshajiang fault is divided into two segments with dextral strike-slip rates of 11.1 ± 0.3 mm/yr and 9.3 ± 0.2 mm/yr.

The Chuandian block contains the Litang, Lijiang–Xiaojinhe, Chenghai, and Yuanmou faults. Earlier field investigations have shown that the Litang fault produces sinistral strike-slip and thrust motion (Xu et al. 2017) with a strike-slip rate of approximately 2.3 mm/yr (Chevalier et al. 2016), which is consistent with the rate of 2.7 ± 0.3 mm/yr determined using our model. The sinistral strike-slip rate of the Lijiang–Xiaojinhe fault is approximately 2.3 mm/yr, which is consistent with that determined by a geological study (Xu et al. 2003). The left-lateral strike-slip Chenghai fault lies southwest of the Lijiang–Xiaojinhe fault. The Chenghai fault plays a key role in regulating the eastward extrusion of material from within the Tibetan Plateau and controls the distribution of strong earthquakes. A previous study showed that the fault has a sinistral strike-slip rate ranging from 2.0 to 4.0 mm/yr (Huang et al. 2018). Our results indicate a slip rate of 1.8 ± 0.4 mm/yr, on the Chenghai fault, which is consistent with previously reported values. The sinistral strike-slip rate of the Yuanmou fault based on geomorphic offset and dating measurements, is approximately 0.45–2.6 mm/yr (Lu et al. 2009), which is slightly lower than the strike-slip rate of 3.2 ± 0.2 mm/yr determined in our study.

Fault slip rates in western Yunnan and eastern Tibet

Southwest of the Red River fault, a series of faults can be divided into two types based on orientation: the Jiali, Nujiang, and Lancangjiang faults trend northwest, and the Longling–Ruili, Nantinghe, and Menglian faults trend northeast. The Jiali fault is the southeastern part of the Karakoram–Jiali dextral strike-slip fault system and has been suggested to be important for regulating crustal deformation and strain partitioning in the southeastern Tibetan Plateau (Tapponnier et al. 2001). The average dextral strike-slip rate

of the Jiali fault is approximately 4 mm/yr (Ren et al. 2000). Our results indicate a right-lateral slip rate of 5.2 ± 0.3 mm/yr for the Jiali fault. We determined an average slip rate of 3.5 ± 0.3 mm/yr for the Lancangjiang fault. This result is lower than the previously reported geologically-based result of approximately 5.3 mm/yr and consistent with the geodesy-based result of 2 ± 2 mm/yr (Xu et al. 2003; Shen et al. 2005). Since the Holocene, the Nantinghe fault has experienced left-lateral strike-slip motion with a well-defined vertical component. The sinistral strike-slip rate of the Nantinghe fault, as determined by geomorphological dislocation and dating, is 3.6 ± 0.4 mm/yr (Sun et al. 2017; Shi et al. 2022), which is slightly greater than the rate of 2.6 ± 0.5 mm/yr determined by our model.

Long-term seismic hazard assessment

Reid (1910) proposed an elastic rebound theory for large, recurring earthquakes and posited quasi-periodic recurrence based on the accumulation and release of seismic energy. By considering the fault slip rate in conjunction with the occurrence of large earthquakes along a fault, we can estimate the seismic hazard by comparing the moment deficit between the moment accumulation and moment release.

Moment accumulation rate

The moment accumulation rate can be calculated by formula $M_f = M_p + M_n$, where $M_p = \mu Ld|v_p|$, and $M_n = \mu Ld|v_n|$, in which μ denotes the shear modulus of the crustal medium, which is usually taken as 3×10^{10} Pa; L denotes the fault length; d denotes the locking depth of the fault, which is equal to that used to calculate the slip rate; v_p denotes the sinistral or dextral strike-slip rate of the fault; and v_n denotes the compressive or tensile rate of the fault.

Moment release

The seismic moment (M_0) released by one earthquake can be estimated by the moment magnitude (M_w): $M_w = (2/3) \log M_0 - 6.03$. Liu et al. (2006) used the orthogonal regression method to determine the relationship between the surface wave magnitude (M_s) and the moment magnitude (M_w) (Liu et al. 2006). As the difference between the two magnitudes is small, the seismic moment release can be approximated by the surface wave magnitude (Wang et al. 2011).

Earthquakes of $M \geq 6.0$ and $M \geq 7.0$ have different complete records, with the latter usually having a longer period than the former. Therefore, the moment release for a fault is obtained by calculating the moment release for earthquakes $7.0 > M \geq 6.0$ and $M \geq 7.0$. The moment release of $M \geq 7.0$

earthquakes can be directly calculated using the aforementioned equation. The moment release of $7.0 > M \geq 6.0$ earthquakes is calculated by using the aforementioned equation and the period of the complete record of $7.0 > M \geq 6.0$ earthquakes. First, the annual mean moment release rate is calculated, and then multiplied by the full recording period of $M \geq 7.0$ earthquakes.

Moment deficit and earthquake hazard assessment

The $M \geq 6.0$ earthquake records for the Sichuan–Yunnan region are complete dating back to A.D. 1900. The complete record of $M \geq 7$ earthquakes varies for different faults (Qin et al. 1999; Huang et al. 2011). According to historical regional strong earthquake data (Department of Earthquake Disaster Prevention, State Seismological Bureau 1995; Department of Earthquake Disaster Prevention, China Earthquake Administration 1999; The Working Group of M7 2012) and modern strong earthquake data (<https://news.ceic.ac.cn/>), relatively complete records have been collected for the $M \geq 7$ and $7.0 > M \geq 6.0$ earthquakes that have occurred on major faults (Fig. 7, Table S3).

The accumulation and release of seismic moments on one fault tend to be balanced during an interseismic period.

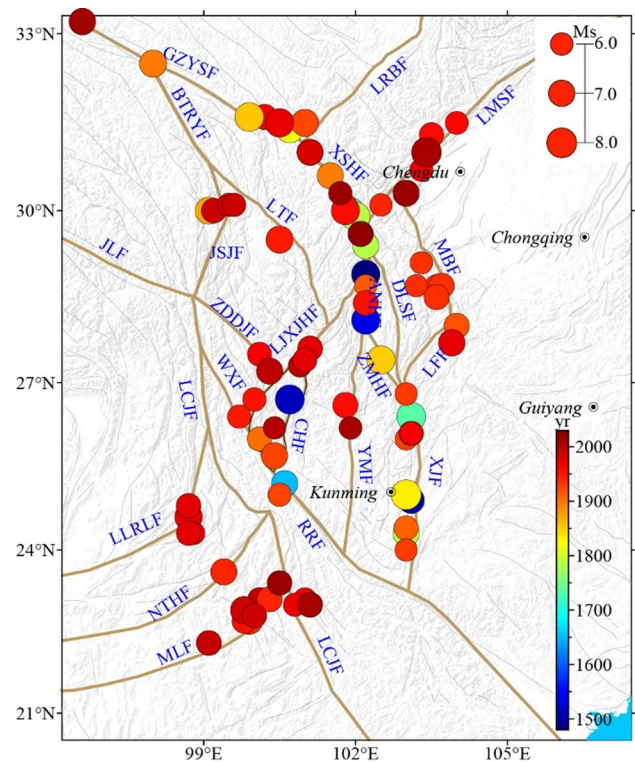


Fig. 7 Earthquakes of $7.0 > M \geq 6.0$ (1900–2022) and the complete record of $M \geq 7.0$ earthquakes along the major faults in the Sichuan–Yunnan region. The fault abbreviations used here are the same as those in Fig. 1

The moment accumulation and moment release for the respective faults were estimated by considering the motion rate, locking depth, active block boundary fault geometric distribution in the Sichuan–Yunnan region, and the strong earthquakes that occurred on each boundary fault (Fig. 8). The moment deficits of the corresponding boundary faults (Fig. 9a) were obtained, and the potential seismic magnitude was calculated by using a seismic moment calculation formula (Fig. 9b). The southern segment of the Xiaojiang fault and the Yuanmou fault were found to have relatively high moment accumulations. The largest moment release occurs in the middle segment of the Longmenshan fault and followed by the northern segment of the Xiaojiang fault. The boundary faults with relatively large moment deficits include the Daliangshan fault (2.89×10^{20} N·m), Longriba fault (2.65×10^{20} N·m), southern segment of the Xiaojiang fault (3.98×10^{20} N·m), Yuanmou fault (2.94×10^{20} N·m), Jiali fault (1.82×10^{20} N·m), and southwestern segment of the Jinshajiang fault (2.28×10^{20} N·m), with corresponding moment magnitudes of M_w 7.6, 7.6, 7.7, 7.6, 7.5, and 7.5 (Fig. 9b). All 19 seismic gaps, except for the Nantinghe and Mabian seismic gaps, are associated with the risk of earthquakes with moment magnitudes larger than 6.5.

Discussion

The fault slip rate refers to the average velocity of a fault dislocation during a specific period (Wallace 1987; Deng et al. 2004). This parameter can reflect the accumulation rate of strain energy for a fault and can be used to quantitatively compare the relative activities of different faults or one fault during different periods. The motion rates of the boundary faults of each subblock were obtained based on the elastic block model (Fig. 6). Most of the slip rates of the boundary faults determined using the block model agree well with those obtained based on geology and chronology through a comparative analysis of the slip rates since the late Quaternary (Fig. 10). Thus, the fault slip rates reported in this paper can essentially represent the long-term motion characteristics of individual faults. Fault motion properties have distinct zoning characteristics. The Sichuan–Yunnan region can be roughly divided into four regions according to the strike-slip motion properties of the boundary faults (Fig. 11a). The Xianshuihe–Xiaojiang fault zone and the secondary faults in the Chuandian block are dominated by left-lateral strike-slip motion; the western Jinshajiang and Zhongdian–Daju faults of the Chuandian block, the Red River fault on the southwest boundary,

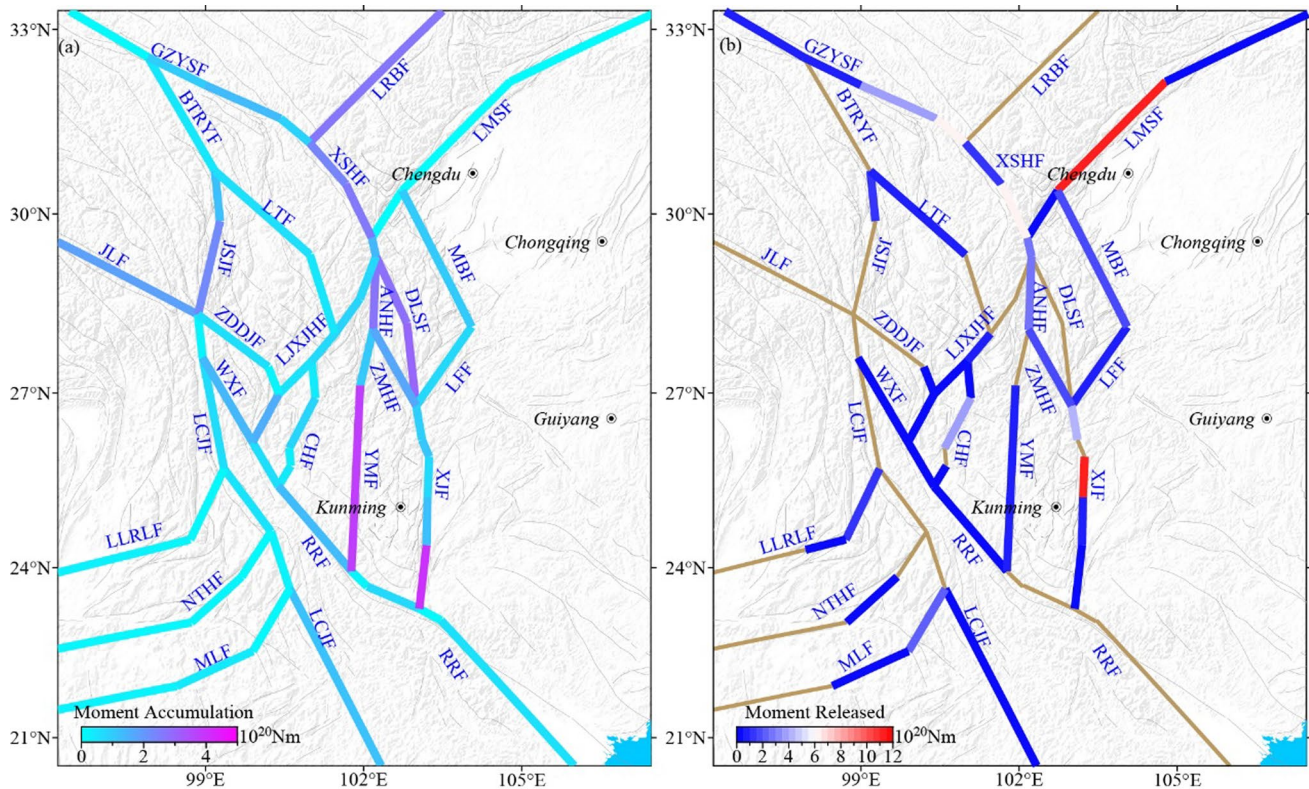


Fig. 8 Long-term moment accumulation (a) and moment release (b). The fault abbreviations used here are the same as those used in Fig. 1

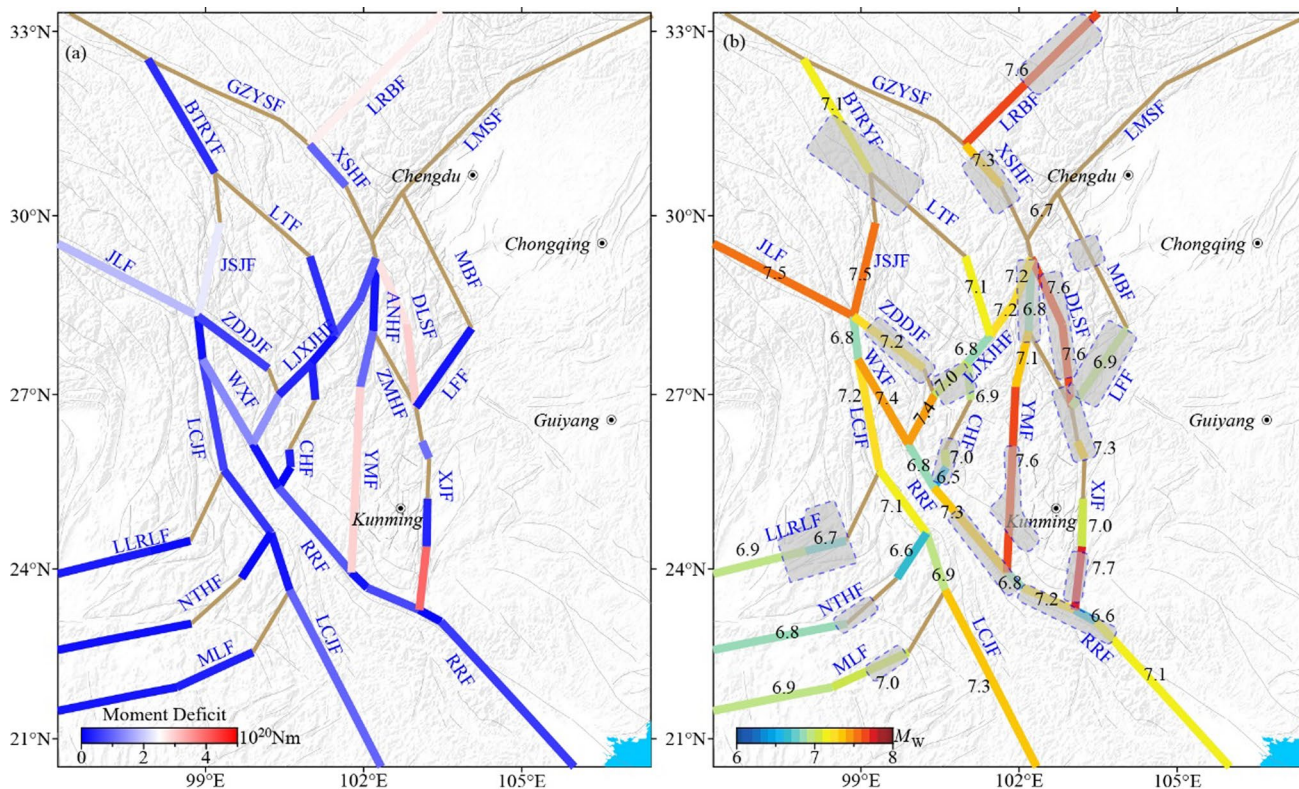


Fig. 9 Moment deficits (a) and predicted moment magnitude (b). The gray area surrounded by dashed lines represents seismic gaps (The Working Group of M7 2012)

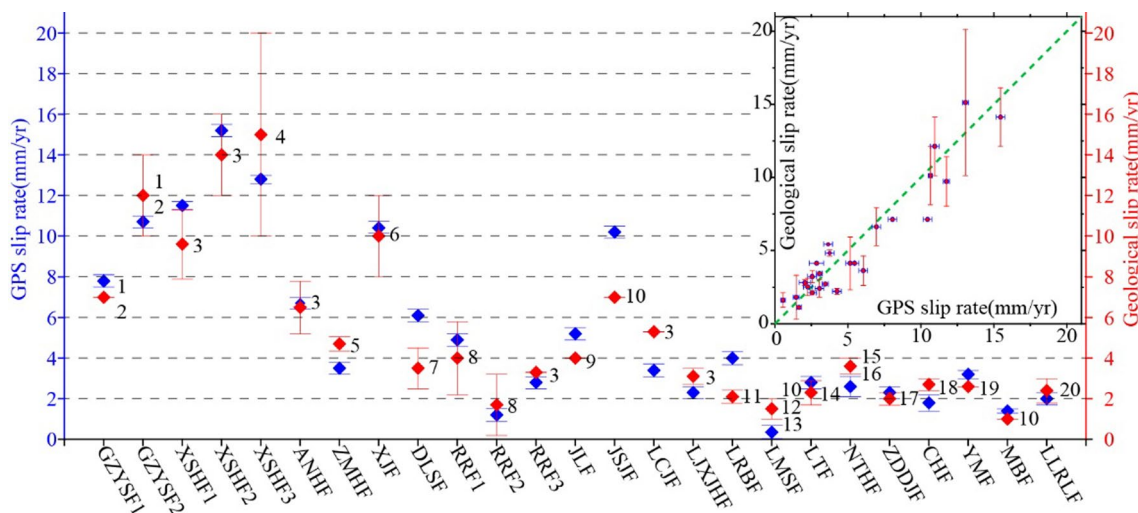


Fig. 10 A comparison of the strike-slip rates of the block model (blue) and previous geological (red) results. The numbers next to the red diamonds represent references as follows: 1 (Wen et al. 2003); 2 (Peng et al. 2006); 3 (Xu et al. 2003); 4 (Allen et al. 1991); 5 (Ren 1994); 6 (Song et al. 1998); 7 (Wei et al. 2012); 8 (Trinh et al. 2012);

9 (Ren et al. 2000); 10 (Tang and Han 1993); 11 (Ren et al. 2013); 12 (Ma et al. 2005); 13 (Zhou et al. 2007); 14 (Chevalier et al. 2016); 15 (Shi et al. 2022); 16 (Sun et al. 2017); 17 (Replumaz and Tapponnier 2003); 18 (Huang et al. 2018); 19 (Lu et al. 2009); and 20 (Huang et al. 2010)

and the Lancangjiang and Jiali faults are dominated by dextral strike-slip motion; the NE-trending Longmenshan and Longriba faults on the east side of the Xianshuihe

fault exhibit prominent dextral strike-slip motion; and the NE-trending faults southwest of the Lancangjiang fault are dominated by sinistral strike-slip motion. Considering

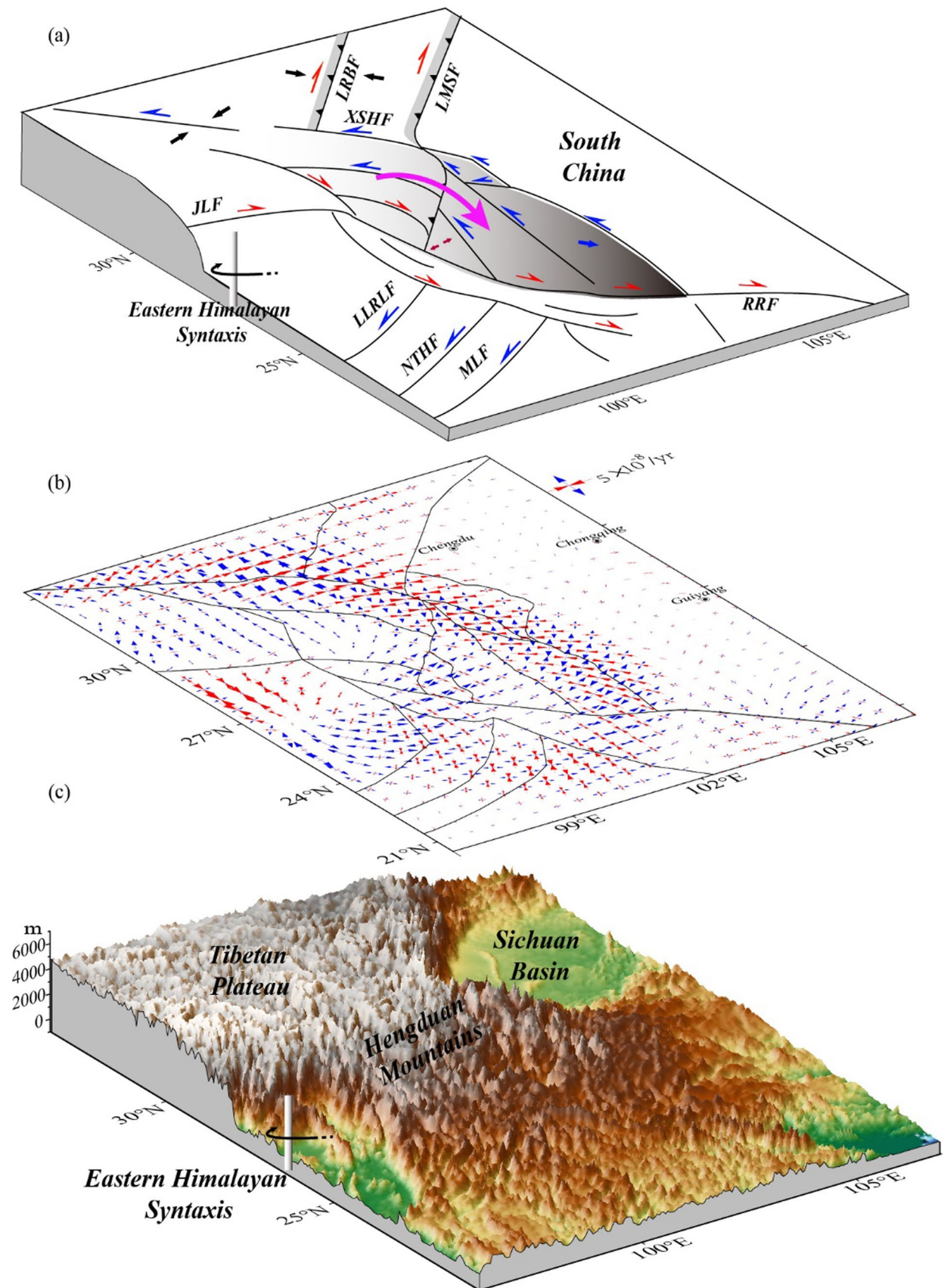


Fig. 11 The strike-slip characteristics of the boundary faults and deformation model for the Sichuan–Yunnan region (a), where the red and blue arrows indicate dextral and sinistral strike-slip motions, respectively. The principal strain rates for the Sichuan–Yunnan region (b), where the red and blue arrows show the principal compressive strain and principal tensile strain, respectively. (c) Sketch of the topography

that the motion properties are perpendicular to the boundary faults, no prominent zoning is observed in the tensile/compressive properties.

The direction of the regional tectonic force acting on a fault is in accord with the principal strain calculated from GNSS data (Chen et al. 2013). The axial direction of the regional compressive strain (Fig. 11b) indicates that the eastern boundary fault of the Chuandian block is subjected to compressive stress in the NW–SE direction, under which the Xianshuihe–Xiaojiang fault zone exhibits clear sinistral strike-slip characteristics. The difference between the motions of adjacent blocks distinctly reflects the magnitude of the boundary fault slip rate (Chen et al. 2013). Figure 4 shows the relative motions between each block and the adjacent blocks. Among the blocks, significantly greater relative motions are found between the Litang subblock and the Maerkang and Aba subblocks on either side of the Xianshuihe fault, between the Dayao and Daliangshan subblocks on either side of the Anninghe fault, between the Yimen and Daliangshan subblocks on either side of the Zemuhe fault, and between the Yimen and Huanan subblocks on either side of the Xiaojiang fault (Fig. 4c, d). The relative motion of these blocks results in the Xianshuihe–Xiaojiang fault zone having a higher slip rate than the other faults.

Under continuous pushing from the Indian plate colliding with the Eurasian plate, the Tibetan Plateau exhibits northward, northeastward, eastward, and southeastward motion and diffusion (Clark and Royden 2000; Zhang et al. 2004; Gan et al. 2007). Many models or hypotheses have been proposed to explain the tectonic deformation and dynamic mechanisms of the plateau, but a consensus has not been reached regarding which model best explains the deformation characteristics. The Sichuan–Yunnan region is located in the area with the most intense eastward extrusion of the Tibetan Plateau. Magnetotelluric imaging results more clearly show lower crustal flow in the Sichuan–Yunnan region than in other regions of the Tibetan Plateau (Zhao et al. 2008; Bai et al. 2010). Shen et al. (2005) proposed that this crustal flow strongly depends on regional crustal deformation. The continuous southward movement of the Qiangtang block, the Bayan Har block, and the subblocks in the Chuandian block from northwest to southeast indicates that the dynamic force of the tectonic deformation in the Sichuan–Yunnan area north of the Red River fault derives from the eastward motion of material in the Tibetan Plateau associated with lower crustal flow. The southward movement

of the Bayan Har block is blocked by the Sichuan Basin which caused the Aba and Maerkang subblocks to rotate clockwise and counterclockwise, respectively. The Jinshajiang fault between the Qiangtang block and the Litang and Daocheng subblocks in the Dianzhong subblock absorbs the eastward slip of the Qiangtang block and transfers the remaining slip to the interior of the Dianzhong subblock, which continues moving eastward. After absorbing the eastward slip of the Litang and Daocheng subblocks, the Xiaojinhe fault in Lijiang transfers the remaining slip to the Chenghai, Dayao, and Yimen subblocks inside the Diannan subblock, and the plateau material migrates southeastward or south southeastward, causing the subblocks in the Diannan subblock to undergo clockwise rotation and southeastern translation. The crustal deformation characteristics, southwest of the Red River fault, are mainly controlled by two large dextral strike-slip faults, i.e., the Red River and Lancangjiang faults (Xu et al. 2003). Nur et al. (1989) proposed a model for the sinistral strike-slip motion of secondary faults under dextral shear deformation and clockwise rotation of the surrounding blocks, which effectively explains the clockwise rotation of the subblocks in the southwest area of the Lancangjiang fault and the sinistral strike-slip motion of the Longling–Ruili and Nantinghe faults (Fig. 11). Combining the analysis results for the motion characteristics of each active block and the motion properties of boundary faults with the characteristics of the regional strain field leads to the conclusion that the crustal deformation in the Sichuan–Yunnan area strongly depends on the eastward or southeastward extrusion of plateau materials, lower crustal flow, and gravitational collapse within the background of the collision between the Indian and Eurasian plates.

Conclusions

The Sichuan–Yunnan region is divided into 17 subblocks based on a comprehensive analysis of various types of data. The slip rate of the boundary fault of each subblock is calculated based on an analysis of the independence and stability of each block, and the medium- and long-term seismic hazards of each fault are investigated. The main conclusions of this study are given below.

1. The F test results, residual distribution characteristics, and RMS error results show that the 17 subblocks are relatively independent. Under clockwise or anticlockwise rotation, each subblock translates to the east, southeast, or southwest. All the subblocks inside the Chuandian block have higher translation rate than the subblocks on either side of this block.
2. The motion properties of the boundary faults in each subblock exhibit distinct zoning characteristics. The

eastern boundary of the Chuandian block and its internal subblocks are dominated by sinistral strike-slip motion, the NW-trending fault east of the Chuandian block is dominated by left-lateral strike-slip motion, and the NE-trending fault is dominated by right-lateral strike-slip movement. In contrast, the southwestern boundary of the Chuandian block and a series of NW-trending faults west of the Chuandian block are dominated by right-lateral strike-slip movement, whereas the NE-trending faults are dominated by left-lateral strike-slip movement. The slip rates of each fault determined using the elastic block model are consistent with those from previous geological studies, and the inversion results represent the long-term motion characteristics of each fault.

3. The most prominent moment deficits for the major faults in the Sichuan–Yunnan region are located along the Daliangshan and Longriba faults, and the southern segments of the Xiaojiang and Yuanmou faults with corresponding moment magnitudes of 7.6, 7.6, 7.6, and 7.7, respectively. Seventeen of the 19 seismic gaps have high seismic moment deficits, and attention should be given to the strong earthquake risks associated with these seismic gaps, especially in the southern segment of the Xiaojiang fault seismic gap.
4. The subblocks in the Sichuan–Yunnan region have clearly different dynamic sources. The subblocks in the region northeast of the Red River fault are primarily caused by the southeastward deflection of plateau material in the process of eastward movement due to blocking of the Sichuan Basin. In contrast, the subblocks southwest of the Lancangjiang fault and the subblocks between the Red River fault and Lancangjiang fault, are affected mainly by the interaction of two large dextral faults.

Supplementary Information The online version contains supplementary material available at <https://doi.org/10.1007/s11600-024-01319-1>.

Acknowledgements The authors would like to thank Dr. Yanqiang Wu and Dr. Peng Wang for their helpful suggestions. Some figures were generated using the Generic Mapping Tools version 6 (Wessel et al. 2019). We thank three anonymous reviewers for their comments which improved this manuscript.

Author contributions CC was involved in conceptualization. XL helped in formal analysis. QZ and SZ contributed to data curation. WZ and CC assisted in writing—original draft preparation. JL and YT assisted in writing—review and editing. NG helped in supervision.

Funding This research was supported by the National Key R & D Program of China (No. 2022YFC3003703) funded by the Ministry of Science, Technology of the People’s Republic of China, the Scientific Research Project Coordinating Fund of the First Monitoring and Application Center, China Earthquake Administration (No. FMC2022014), and the Earthquake Tracking Track of China Earthquake Administration (No. CEA; 2023010219).

Declarations

Conflict of interest The authors declare no conflicts of interest.

References

- Allen CR, Gillespie AR, Han Y et al (1984) Red River and associated faults, Yunnan Province, China: quaternary geology, slip rates, and seismic hazard. *GSA Bull* 95:686–700. [https://doi.org/10.1130/0016-7606\(1984\)95%3c686:RRAAFY%3e2.0.CO;2](https://doi.org/10.1130/0016-7606(1984)95%3c686:RRAAFY%3e2.0.CO;2)
- Allen CR, Luo Z, Qian H et al (1991) Field study of a highly active fault zone: the Xianshuihe fault of southwestern China. *GSA Bull* 103:1178–1199. [https://doi.org/10.1130/0016-7606\(1991\)103%3c1178:FSOAHA%3e2.3.CO;2](https://doi.org/10.1130/0016-7606(1991)103%3c1178:FSOAHA%3e2.3.CO;2)
- Armijo R, Tapponnier P, Han T (1989) Late Cenozoic right-lateral strike-slip faulting in southern Tibet. *J Geophys Res Solid Earth* 94:2787–2838. <https://doi.org/10.1029/JB094iB03p02787>
- Bai D, Unsworth MJ, Meju MA et al (2010) Crustal deformation of the eastern Tibetan plateau revealed by magnetotelluric imaging. *Nat Geosci* 3:358–362. <https://doi.org/10.1038/ngeo830>
- Botsyo S, Bortei BB, Ayer J (2020) CORS usage for GPS survey in the Greater Accra region: advantages, limitation, and suggested remedies. *J Geovis Spat Anal* 4:20. <https://doi.org/10.1007/s41651-020-00061-8>
- Bureau of Geology and Mineral Resources of Yunnan Province (1990) Regional geology of Yunnan province. Geological Publishing House, Beijing
- Chang L, Flesch LM, Wang C-Y, Ding Z (2015) Vertical coherence of deformation in lithosphere in the eastern Himalayan syntaxis using GPS, quaternary fault slip rates, and shear wave splitting data. *Geophys Res Lett* 42:5813–5819. <https://doi.org/10.1002/2015GL064568>
- Chen C, Ren J, Meng G et al (2013) Division, deformation and tectonic implication of active blocks in the eastern segment of Bayan Har block. *Chinese J Phys* 56:4125–4141. <https://doi.org/10.6038/cjg20131217>
- Cheng J, Xu X, Gan W et al (2012) Block model and dynamic implication from the earthquake activities and crustal motion in the southeastern margin of Tibetan plateau. *Chinese J Phys* 55:1198–1212. <https://doi.org/10.6038/J.ISSN.0001-5733.2012.04.016>
- Chevalier M-L, Leloup PH, Replumaz A et al (2016) Tectonic-geomorphology of the Litang fault system, SE Tibetan plateau, and implication for regional seismic hazard. *Tectonophysics* 682:278–292. <https://doi.org/10.1016/j.tecto.2016.05.039>
- Clark MK, Royden LH (2000) Topographic ooze: building the eastern margin of Tibet by lower crustal flow. *Geology* 28:703–706. [https://doi.org/10.1130/0091-7613\(2000\)28%3c703:TOBTEM%3e2.0.CO;2](https://doi.org/10.1130/0091-7613(2000)28%3c703:TOBTEM%3e2.0.CO;2)
- Deng Q, Chen L, Ran Y (2004) Quantitative studies and applications of active tectonics. *Earth Sci Front* 11:383–392
- Densmore AL, Ellis MA, Li Y et al (2007) Active tectonics of the Beichuan and Pengguan faults at the eastern margin of the Tibetan plateau. *Tectonics*. <https://doi.org/10.1029/2006TC001987>
- Department of Earthquake Disaster Prevention, State Seismological Bureau (1995) The catalogue of Chinese historical strong earthquakes. Seismological Press, Beijing
- Department of Earthquake Disaster Prevention, China Earthquake Administration (1999) The catalogue of Chinese modern earthquakes. China Science and Technology Press, Beijing
- England P, Molnar P (2005) Late quaternary to decadal velocity fields in Asia. *J Geophys Res Solid Earth*. <https://doi.org/10.1029/2004JB003541>

- Fielding EJ (1996) Tibet uplift and erosion. *Tectonophysics* 260:55–84. [https://doi.org/10.1016/0040-1951\(96\)00076-5](https://doi.org/10.1016/0040-1951(96)00076-5)
- Gan W, Zhang P, Shen Z-K et al (2007) Present-day crustal motion within the Tibetan plateau inferred from GPS measurements. *J Geophys Res Solid Earth*. <https://doi.org/10.1029/2005JB004120>
- He H, Oguchi T (2008) Late quaternary activity of the Zemuhe and Xiaojiang faults in southwest China from geomorphological mapping. *Geomorphology* 96:62–85. <https://doi.org/10.1016/j.geomorph.2007.07.009>
- He H, Ran H, Ikeda Y (2006) Uniform strike-slip rate along the Xianshuihe-Xiaojiang fault system and its implications for active tectonics in Southeastern Tibet. *Acta Geol Sin* 80:376–386
- He H, Ikeda Y, He Y et al (2008) Newly-generated Daliangshan fault zone—shortcutting on the central section of Xianshuihe-Xiaojiang fault system. *Sci China Ser D-Earth Sci* 51:1248–1258. <https://doi.org/10.1007/s11430-008-0094-4>
- Huang X, Du Y, Shu S, Xie F (2010) Study of the late quaternary slip rate along the northern segment on the south branch of Longling-Ruilu fault. *Seismol Geol* 32:222–232
- Huang W, Li W, Cao X (2011) Research on the completeness of earthquake data in the Chinese mainland (II). *Acta Geol Sin* 16:423–432
- Huang X, Wu Z, Huang X, Luo R (2018) Tectonic geomorphology constrains on quaternary activity and segmentation along Chenghai-Binchuan fault zone in Northwest Yunnan China. *Earth Sci* 43:4651–4670
- Kong F, Wen K, Li Y (2019) Regularized multiple sparse Bayesian learning for hyperspectral target detection. *J Geovis Spat Anal* 3:11. <https://doi.org/10.1007/s41651-019-0034-1>
- Kreemer C, Blewitt G, Klein EC (2014) A geodetic plate motion and global strain rate model. *Geochem Geophys Geosyst* 15:3849–3889. <https://doi.org/10.1002/2014GC005407>
- Lee T-Y, Lawver LA (1995) Cenozoic plate reconstruction of Southeast Asia. *Tectonophysics* 251:85–138. [https://doi.org/10.1016/0040-1951\(95\)00023-2](https://doi.org/10.1016/0040-1951(95)00023-2)
- Li C, Pang J, Zhang Z (2012) Characteristics, geometry, and segmentation of the surface rupture associated with the 14 April 2010 Yushu earthquake, Eastern Tibet, China. *Bull Seismol Soc Am* 102:1618–1638. <https://doi.org/10.1785/0120110261>
- Li Y, Hao M, Song S et al (2021) Interseismic fault slip deficit and coupling distributions on the Anninghe-Zemuhe-Daliangshan-Xiaojiang fault zone, southeastern Tibetan plateau, based on GPS measurements. *J Asian Earth Sci* 219:104899. <https://doi.org/10.1016/j.jseae.2021.104899>
- Liang S, Gan W, Shen C et al (2013) Three-dimensional velocity field of present-day crustal motion of the Tibetan plateau derived from GPS measurements. *J Geophys Res Solid Earth* 118:5722–5732. <https://doi.org/10.1002/2013JB010503>
- Liu R, Chen Y, Bormann P et al (2006) Comparison between earthquake magnitudes determined by China seismograph network and US seismograph network (II): surface wave magnitude. *Acta Seismol Sin* 19:1–7
- Liu B, Peng T, Fan W et al (2020) Tectonic evolution and Paleoposition of the Baoshan and Lincang blocks of West Yunnan during the Paleozoic. *Tectonics* 39:e2019TC006028. <https://doi.org/10.1029/2019TC006028>
- Liu R, Yang C, Wang Q et al (2021) Possible mechanism of the formation of the Jichechang ground fissure in Datong, China, based on in-situ observations. *Environ Earth Sci* 8(25):4333–4338. <https://doi.org/10.1007/s12665-021-09715-2>
- Loveless JP, Meade BJ (2011) Partitioning of localized and diffuse deformation in the Tibetan plateau from joint inversions of geologic and geodetic observations. *Earth Planet Sci Lett* 303:11–24. <https://doi.org/10.1016/j.epsl.2010.12.014>
- Lu H, Wang R, Zhao J et al (2009) Tectonic activities of the Yuanmou fault in late quaternary and analysis of its tectonic stress. *Quat Sci* 29:173–182. <https://doi.org/10.3969/j.issn.1001-7410.2009.01.20>
- Ma B, Su G, Hou Z, Shu S (2005) Late quaternary slip rate in the central part of the Longmenshan fault zone from terrace deformation along the Minjiang river. *Seismol Geol* 27:234
- Meade BJ (2007) Present-day kinematics at the India-Asia collision zone. *Geology* 35:81–84. <https://doi.org/10.1130/G22924A.1>
- Meade BJ, Loveless JP (2009) Block modeling with connected fault-network geometries and a linear elastic coupling estimator in spherical coordinates. *Bull Seismol Soc Am* 99:3124–3139. <https://doi.org/10.1785/0120090088>
- Nur A, Ron H, Scotti O (1989) Kinematics and mechanics of Tectonic block rotations. *Slow Deform Transm Stress Earth* 49:31–46
- Okada Y (1985) Surface deformation due to shear and tensile faults in a half-space. *Bull Seismol Soc Am* 75:1135–1154. <https://doi.org/10.1785/BSSA0750041135>
- Peng H, Ma X, Bai J, Du D (2006) Characteristics of quaternary activities of the Ganzê-Yushu fault zone. *J Geomechanics* 12:295–304
- Qin C, Papadimitriou EE, Papazachos BC, Karakaisis GF (1999) Spatial distribution of time-independent seismicity in China. *Pure Appl Geophys* 154:101–119. <https://doi.org/10.1007/s000240050223>
- Reid H (1910) The mechanism of the earthquake, in the California earthquake of April 18, 1906. Report of the state earthquake investigation commission. vol. 2, pp 16–28
- Ren J (1994) Late quaternary displacement and slip rate of Zemuhe fault in Sichuan. *China Seismol Geol* 16:146
- Ren J, Shen J, Cao Z, Wang Y (2000) Quaternary faulting of Jiali fault, southeast Tibetan plateau. *Seismol Geol* 22:344
- Ren J, Xu X, Yeats RS, Zhang S (2013) Latest quaternary paleoseismology and slip rates of the Longriba fault zone, eastern Tibet: implications for fault behavior and strain partitioning. *Tectonics* 32:216–238. <https://doi.org/10.1002/tect.20029>
- Replumaz A, Tapponnier P (2003) Reconstruction of the deformed collision zone between India and Asia by backward motion of lithospheric blocks. *J Geophys Res Solid Earth*. <https://doi.org/10.1029/2001JB000661>
- Savage JC, Burford RO (1973) Geodetic determination of relative plate motion in central California. *J Geophys Res Solid Earth* 78:832–845. <https://doi.org/10.1029/JB078i005p00832>
- Shen S, Shi GR, Zongjie F (2002) Permian brachiopods from the Baoshan and Simao blocks in Western Yunnan, China. *J Asian Earth Sci* 20:665–682. [https://doi.org/10.1016/S1367-9120\(01\)00062-1](https://doi.org/10.1016/S1367-9120(01)00062-1)
- Shen Z-K, Lü J, Wang M, Bürgmann R (2005) Contemporary crustal deformation around the southeast borderland of the Tibetan plateau. *J Geophys Res Solid Earth*. <https://doi.org/10.1029/2004JB003421>
- Shi F, He H, Liu Y et al (2022) Active tectonics of the Nantinghe fault in Southeastern Tibetan plateau and its Implications for Continental collision. *Front Earth Sci*. <https://doi.org/10.3389/feart.2021.818225>
- Song F, Wang Y, Yu W et al (1998) Xiaojiang active fault belt. Seismological Press, Beijing
- Su X, Shi R, Bao Q et al (2023) Self-adaptive extraction method of tectonic movement change recorded by GNSS continuous observation. *Acta Geodaet Cartographica Sin* 52:1245–1254. <https://doi.org/10.11947/j.AGCS.2023.20220675>
- Sun H, He H, Wei Z et al (2017) Late Quaternary paleoearthquakes along the northern segment of the Nantinghe fault on the southeastern margin of the Tibetan plateau. *J Asian Earth Sci* 138:258–271. <https://doi.org/10.1016/j.jseae.2017.02.023>
- Tang R, Han W (1993) Active faults and earthquakes in Sichuan Province. Seismological Press, Beijing

- Tao Y, Liu C, Liu C et al (2021) Empirical wavelet transform method for GNSS coordinate series denoising. *J Geovisualization Spat Anal* 5(1):9. <https://doi.org/10.1007/s41651-021-00078-7>
- Tapponnier P, Lacassin R, Leloup PH et al (1990) The Ailao Shan/Red river metamorphic belt: tertiary left-lateral shear between Indochina and South China. *Nature* 343:431–437. <https://doi.org/10.1038/343431a0>
- Tapponnier P, Zhiqin X, Roger F et al (2001) Oblique stepwise rise and growth of the Tibet plateau. *Science* 294:1671–1677. <https://doi.org/10.1126/science.105978>
- The Working Group of M7 (2012) Study on the mid- to long-term potential of large earthquakes on the Chinese continent, 1st edn. Seismological Press, Beijing
- Trinh PT, Liem NV, Huong NV et al (2012) Late quaternary tectonics and seismotectonics along the Red river fault zone, North Vietnam. *Earth Sci Rev* 114:224–235. <https://doi.org/10.1016/j.earscirev.2012.06.008>
- Wallace RE (1987) Grouping and migration of surface faulting and variations in slip rates on faults in the Great Basin province. *Bull Seismol Soc Am* 77:868–876. <https://doi.org/10.1785/BSSA0770030868>
- Wang E (1998) Late cenozoic Xianshuihe-Xiaojiang, Red river, and Dali fault systems of Southwestern Sichuan and Central Yunnan. Geological Society of America, China
- Wang M, Shen Z-K (2020) Present-day crustal deformation of continental China derived from GPS and its tectonic implications. *J Geophys Res Solid Earth* 125:e2019JB018774. <https://doi.org/10.1029/2019JB018774>
- Wang Q, Zhang P-Z, Freymueller JT et al (2001) Present-day crustal deformation in China constrained by global positioning system measurements. *Science* 294:574–577. <https://doi.org/10.1126/science.1063647>
- Wang M, Shen Z, Niu Z et al (2003) Contemporary crustal deformation of the Chinese continent and tectonic block model. *Sci China Ser D-Earth Sci* 46:25–40. <https://doi.org/10.1360/03dz0003>
- Wang Y, Wang E, Shen Z et al (2008) GPS-constrained inversion of present-day slip rates along major faults of the Sichuan-Yunnan region, China. *Sci China Ser D-Earth Sci* 51:1267–1283. <https://doi.org/10.1007/s11430-008-0106-4>
- Wang H, Wright TJ, Biggs J (2009) Interseismic slip rate of the northwestern Xianshuihe fault from InSAR data. *Geophys Res Lett.* <https://doi.org/10.1029/2008GL036560>
- Wang H, Liu M, Cao J et al (2011) Slip rates and seismic moment deficits on major active faults in mainland China. *J Geophys Res Solid Earth.* <https://doi.org/10.1029/2010JB007821>
- Wang Y, Wang M, Shen Z-K (2017) Block-like versus distributed crustal deformation around the northeastern Tibetan plateau. *J Asian Earth Sci* 140:31–47. <https://doi.org/10.1016/j.jseas.2017.02.040>
- Wang W, Qiao X, Ding K (2021) Present-Day Kinematics in Southeastern Tibet Inferred from GPS measurements. *J Geophys Res Solid Earth* 126:e2020JB021305. <https://doi.org/10.1029/2020JB021305>
- Wang J, Xu C, Wen Y et al (2022) Characteristics of segmentation and interseismic coupling along the red river fault from GPS observations. *Chinese J Phys* 65:1240–1254. <https://doi.org/10.6038/cjg2022P0174>
- Wei Z, He H, Shi F et al (2012) Slip rate on the south segment of Daliangshan fault zone. *Seismol Geol* 34:282–293
- Wen X, Xu X, Zheng R et al (2003) Average slip-rate and recent large earthquake ruptures along the Garzê-Yushu fault. *Sci China Ser D-Earth Sci* 46:276–288. <https://doi.org/10.1360/03dz0022>
- Wen X, Zhang P, Du F, Long F (2009) The background of historical and modern seismic activities of the occurrence of the 2008 Ms8.0 Wenchuan, Sichuan, earthquake. *Chinese J Phys* 52:444–454
- Wen X, Du F, Zhang P, Long F (2011) Correlation of major earthquake sequences on the northern and eastern boundaries of the Bayan Har block, and its relation to the 2008 Wenchuan earthquake. *Chinese J Phys* 54:706–716. <https://doi.org/10.3969/j.issn.0001-5733.2011.03.010>
- Wessel P, Luis JF, Uieda L et al (2019) The generic mapping tools version 6. *Geochem Geophys Geosyst* 20:5556–5564. <https://doi.org/10.1029/2019GC008515>
- Wu Y, Jiang Z, Zhao J et al (2015) Crustal deformation before the 2008 Wenchuan MS8.0 earthquake studied using GPS data. *J Geodyn* 85:11–23. <https://doi.org/10.1016/j.jog.2014.12.002>
- Xiang H, Guo S, Xu X et al (2000) Active block division and present-day motion features of the south region of Sichuan-Yunnan province. *Seismol Geol* 22:253–264
- Xu X, Wen X, Zheng R et al (2003) Pattern of latest tectonic motion and its dynamics for active blocks in Sichuan-Yunnan region, China. *Sci China Ser D-Earth Sci* 46:210–226. <https://doi.org/10.1360/03dz0017>
- Xu X, Wen X, Chen G, Yu G (2008) Discovery of the Longriba fault zone in eastern Bayan Har block, China and its tectonic implication. *Sci China Ser D-Earth Sci* 51:1209–1223. <https://doi.org/10.1007/s11430-008-0097-1>
- Xu X, Wu Y, Yu G et al (2017) Features of active tectonics and recurrence behaviors of strong earthquakes in the western Sichuan province and its adjacent regions. *Seismol Geol* 39:219. <https://doi.org/10.3969/j.issn.0253-4967.2017.02.001>
- Yan D, Li S, Cao W, Zhang W (2010) Multi-layer detachment crustal structure in the Longmen mountains: evidences from neo-tectonic deformation and geophysical data. *Earth Sci Front* 17:106–116
- Yi G, Long F, Liang M et al (2017) Focal mechanism solutions and seismogenic structure of the 8 August 2017 M7.0 Jiuzhaigou earthquake and its aftershocks, northern Sichuan. *Chinese J Phys* 60:4083–4097. <https://doi.org/10.6038/cjg20171033>
- Zhang P, Deng Q, Zhang G et al (2003) Active tectonic blocks and strong earthquakes in the continent of China. *Sci China Ser D-Earth Sci* 46:13–24. <https://doi.org/10.1360/03dz0002>
- Zhang P, Shen Z, Wang M et al (2004) Continuous deformation of the Tibetan plateau from global positioning system data. *Geology* 32:809–812. <https://doi.org/10.1130/G20554.1>
- Zhang P, Xu X, Wen X, Ran Y (2008) Slip rates and recurrence intervals of the longmen shan active fault zone, and tectonic implications for the mechanism of the May 12 Wenchuan earthquake, 2008, Sichuan, China. *Chinese J Phys* 51:1066–1073
- Zhao G, Chen X, Wang L et al (2008) Evidence of crustal ‘channel flow’ in the eastern margin of Tibetan plateau from MT measurements. *Chin Sci Bull* 53:1887–1893. <https://doi.org/10.1007/s11434-008-0081-3>
- Zhao J, Ren J, Liu J et al (2020) Coupling fraction and relocking process of the longmenshan fault zone following the 2008 Mw7.9 Wenchuan earthquake. *J Geodyn* 137:101730. <https://doi.org/10.1016/j.jog.2020.101730>
- Zheng G, Wang H, Wright TJ et al (2017) Crustal deformation in the India-Eurasia collision zone from 25 years of GPS measurements. *J Geophys Res Solid Earth* 122:9290–9312. <https://doi.org/10.1002/2017JB014465>
- Zhou R, Li Y, Densmore AL et al (2007) Active tectonics of the longmen Shan region on the Eastern margin of the Tibetan plateau. *Acta Geol Sin* 81:593–604. <https://doi.org/10.1111/j.1755-6724.2007.tb00983.x>

Springer Nature or its licensor (e.g. a society or other partner) holds exclusive rights to this article under a publishing agreement with the author(s) or other rightsholder(s); author self-archiving of the accepted manuscript version of this article is solely governed by the terms of such publishing agreement and applicable law.